AGU PUBLICATIONS

JGR

Journal of Geophysical Research: Oceans

RESEARCH ARTICLE

10.1002/2015JC011300

**Key Points:**

- The residence time of mobile mud in East China Sea is estimated to vary between 3 and 6 years
- The mean thickness of mobile varies seasonally
- $^{137}$Cs is tracer of mobile mud in the river-dominated estuaries and coastal areas around the world

**Supporting Information:**

- Supporting Information S1

**Correspondence to:**
J. Du,
jzdu@sklec.ecnu.edu.cn

**Citation:**
Wang, J., J. Du, M. Baskaran, and J. Zhang (2016), Mobile mud dynamics in the East China Sea elucidated using $^{210}$Pb, $^{137}$Cs, $^{7}$Be, and $^{234}$Th as tracers, *J. Geophys. Res. Oceans*, *121*, 224–239, doi:10.1002/2015JC011300.

Received 8 SEP 2015
Accepted 7 DEC 2015
Accepted article online 13 DEC 2015
Published online 10 JAN 2016



# Mobile mud dynamics in the East China Sea elucidated using $^{210}$Pb, $^{137}$Cs, $^{7}$Be, and $^{234}$Th as tracers

**Jinlong Wang[1], Jinzhou Du[1], Mark Baskaran[2], and Jing Zhang[1]**

[1]State Key Laboratory of Estuarine and Coastal Research, East China Normal University, Shanghai, People's Republic of China, [2]Department of Geology, Wayne State University, Detroit, Michigan, USA

**Abstract** "Mobile mud" (MM), which has fine grain size distribution (>90% clay + silt, and <5% sand) and high porosity (≥0.50), plays an important role in the biogeochemical cycles in the estuarine areas and the inshore shelf. A suite of MM samples from the coastal area of the East China Sea (ECS) was collected in spring and summer of 2011 to observe their spatial and temporal distribution, grain size, and radionuclides concentrations. The MM thickness ranged from 0.5 to 11 cm (average: 2.2 cm (May) and 3.9 cm (August)). The thick mud layer is mainly distributed along the coast, with an area of $2.2 \times 10^4$ km$^2$ in May and $1.5 \times 10^4$ km$^2$ in August, with corresponding masses of $8.8 \times 10^8$ and $7.8 \times 10^8$ t, respectively. The estimated masses of MM are considerably larger than the annual sediment discharge mass of the Changjiang River. The distribution of $^{137}$Cs inventories in MM indicates that $^{137}$Cs can be effectively utilized as a transport tracer of MM in the river-dominated estuaries and coastal areas. The higher inventories of $^{7}$Be in MM in the river mouth in spring are attributed to higher depositional flux and higher sediment discharge. The ratio of the MM inventory of $^{234}$Th$_{ex}$/production in the overlying water column of >2.5 in south inshore indicates that the sediment focusing resulted in the increased mass flux. The residence time of MM is estimated as 3–6 years both by mass balance of MM and $^{210}$Pb$_{ex}$ in MM.

## 1. Introduction

In the coastal and shelf areas of River-Dominated Ocean Margins (RiOMars) system, "mobile mud" (MM), mainly comprised of sedimentary particles, with a size of ≤63 $\mu$m and high water content (≥50%), plays a major role in the transport, deposition, and eventual burial of river-derived sedimentary material and associated particle-reactive species [*DeMaster et al.*, 1986; *Milliman*, 1991; *Kineke and Sternberg*, 1995; *Aller*, 1998]. Due to physical (e.g., waves and tide-generated currents) and biological (bioturbation) forcing, the sedimentary particulate matter may undergo several cycles of deposition-resuspension-transport processes in which the sorption/desorption of key micro and macronutrients and other redox-sensitive trace species could impact the biogeochemical cycling in the coastal and shelf areas [*Aller*, 1998; *Aller et al.*, 2004]. Resuspension followed by advective transport of MM associated with storms and heavy winds will result in the advective transport of pore water that is enriched with key nutrients, such as nitrogen, phosphorus, and carbon, into the water column, thus altering the biogeochemistry of these elements [*Giffin and Corbett*, 2003]. These sedimentary materials are primarily derived from the resuspension of the upper 20–200 cm, depending on the existing dynamic system at the river mouth (e.g., upper ~200 cm in the Amazon river mouth [*Aller et al.*, 2004], ~12 cm in the Mississippi River mouth [*Corbett et al.*, 2004], and ~100 cm in Papua Gulf [*Bianchi et al.*, 2007]), estuarine circulation, tidal currents, coastal upwelling, and the intensity of precipitation from monsoons and typhoons. The deposition and subsequent resuspension of MM also affects the redox cycling of various elements such as Fe and Mn, as well the remineralization of sedimentary organic material [*Aller*, 1998].

The East China Sea (ECS) is a typical River-Dominated Ocean Margin system, receiving approximately $3.5 \times 10^8$ t yr$^{-1}$ of terrestrial sediment from the Changjiang River [*Yang et al.*, 2005]. Due to the construction of impoundments, the sediment delivery via the Changjiang River to the ECS has decreased by ~40% since 2000 (from $3.5 \times 10^8$ t yr$^{-1}$ in 2000 to $2.0 \times 10^8$ t yr$^{-1}$ in 2011) [*Yang et al.*, 2005; *Ministry of Water Resources Changjiang Water Resources Commission*, 2011; *Dai and Liu*, 2013]. The differences in the long-term (<1–5 cm yr$^{-1}$) and short-term (~4 cm month$^{-1}$) sedimentation rates indicate that a major proportion of the river-derived sediment is eroded on a seasonal basis (i.e., winter) and transported farther offshore, presumably southward along the coasts of Zhejiang and Fujian Provinces, reaching the Taiwan Strait [*McKee et al.*, 1983; *Su and Huh*, 2002; *Liu et al.*, 2007]. As a direct and quick response to the sharp decreases of the riverine sediment discharge into the Changjiang estuary, the present delta evolution has changed from rapidly accretionary to slow advancement, and even local regions have seen erosion [*Yang et al.*, 2003, 2005; *Dai et al.*, 2014a]. The majority of existing studies have been granulometric parameter studies of muddy sediments, studies on the deposition rate, geochemistry, redox studies, etc. [*Huh and Su*, 1999; *Zhang et al.*, 2005; *Zhu et al.*, 2011; *Dai et al.*, 2014b], whereas less attention has been given to the formation and transport mechanisms of MM, particularly in the Changjiang River estuary and the dynamic processes in the ECS shelf area.

Due to their particle affinity, several naturally occurring and anthropogenic radionuclides, such as $^{234}$Th, $^{7}$Be, $^{210}$Pb, and $^{137}$Cs, can be broadly utilized to investigate the dynamics of suspended particles and sediments in estuarine, coastal, and marine environments [e.g., *DeMaster et al.*, 1986; *Baskaran et al.*, 1997; *Huh and Su*, 1999; *Feng et al.*, 1999; *Du et al.*, 2010; *Huang et al.*, 2013]. $^{234}$Th ($T_{1/2} = 24.1$ days) is continuously produced in seawater from the alpha decay of its parent $^{238}$U and is easily hydrolyzed. $^{234}$Th, which has a high particle reactivity ($K_d \sim 10^4-10^7$ cm$^3$ g$^{-1}$) is a powerful tracer for the investigation of particle/sediment mixing/deposition/reworking processes on weekly to monthly time scales (seasonal variations) in estuaries, coastal ocean, and continental margins [*Smoak et al.*, 2000; *Huang et al.*, 2012]. $^{7}$Be ($T_{1/2} = 53.3$ days) is produced from the cosmic ray spallation reactions of bombardment of nitrogen or oxygen in the atmosphere, scavenged by the atmospheric aerosols and is transported to Earth's surface through wet and dry atmospheric deposition (mainly by wet deposition) [*Du et al.*, 2008]. Once transported to the surface waters, $^{7}$Be is rapidly adsorbed onto particle surfaces ($K_d = 10^4-10^6$ cm$^3$ g$^{-1}$) [*Kaste and Baskaran*, 2011] in aquatic systems and subsequently removed from the water column in coastal environments. $^{7}$Be is widely used as a short-term tracer for sediment accumulation and mixing rates and to quantify sediment resuspension rates in aquatic environments [*Feng et al.*, 1999; *Fitzgerald et al.*, 2001; *Jweda et al.*, 2008; *Du et al.*, 2010]. $^{210}$Pb ($T_{1/2} = 22.3$ year) is one of the decay products in the $^{238}$U-series and is primarily derived from atmospheric deposition when $^{222}$Rn that escapes from Earth's surface undergoes radioactive decay in the atmosphere. Since 1952, $^{137}$Cs ($T_{1/2} = 30.1$ year) has been primarily introduced to the environment from thermonuclear bomb testing, with the maximum number of nuclear tests conducted in 1962. $^{137}$Cs has also become a useful tracer to study the soil erosion and sediment deposition rate in freshwater systems [*Corbett et al.*, 2004; *Hideshi et al.*, 2007]. This suite of four radionuclides ($^{234}$Th, $^{7}$Be, $^{210}$Pb, and $^{137}$Cs) is widely used as particle tracers on time scales of a few days to ~100 years to evaluate spatial and temporal trends in sediment deposition and sediment dynamics.

In our previous work, using a mass balance approach in two-dimensional models, we calculated the removal times of $^{7}$Be, $^{210}$Pb, and $^{234}$Th in the Changjiang River mouth and reported that the removal and resuspension fluxes were comparable in the estuary [*Huang et al.*, 2013]. Based on the mass balance, we also calculated that ~35% of the total $^{210}Pb_{ex}$ and $^{7}$Be inputs into the Changjiang estuary should be exported out of this area [*Du et al.*, 2010]. In the present work, we extended our research to focus on the movement of MM in the Changjiang estuary and ECS using a set of radionuclides to evaluate the temporal and spatial distribution of MM in the study area. This study represents the first attempt to evaluate the short-term (seasonal) MM dynamics in the Changjiang River deltaic region. The results are expected to promote our understanding of not only the processes of sediment deposition/reworking in estuarine and continental shelf areas but also the processes of biogeochemical cycles of biogenic elements in estuarine and continental shelf areas.

## 2. Materials and Methods

### 2.1. Study Area

The ECS, with total area of $7.7 \times 10^5$ km$^2$, is ~400 km long and has a maximum width of ~640 km, with an average water depth of 72 m. The topography of the ECS slants gently from the continental shelf toward the southeast (average gradient: 0.04%). The region to the east of the 50–60 m isobath is the outer continental shelf, which has a flat terrain. An ~800 km long mud area exists on the south coast of the Changjiang River and extends to the northern Taiwan Strait [*Liu et al.*, 2007]. The clinoform is thickest (40 m) between the 20 and 30 m isobaths and becomes progressively thinner offshore, reaching water depths of 60 and 90 m and distances of up to 100 km offshore [*Liu et al.*, 2006]. Four sedimentary facies have been defined

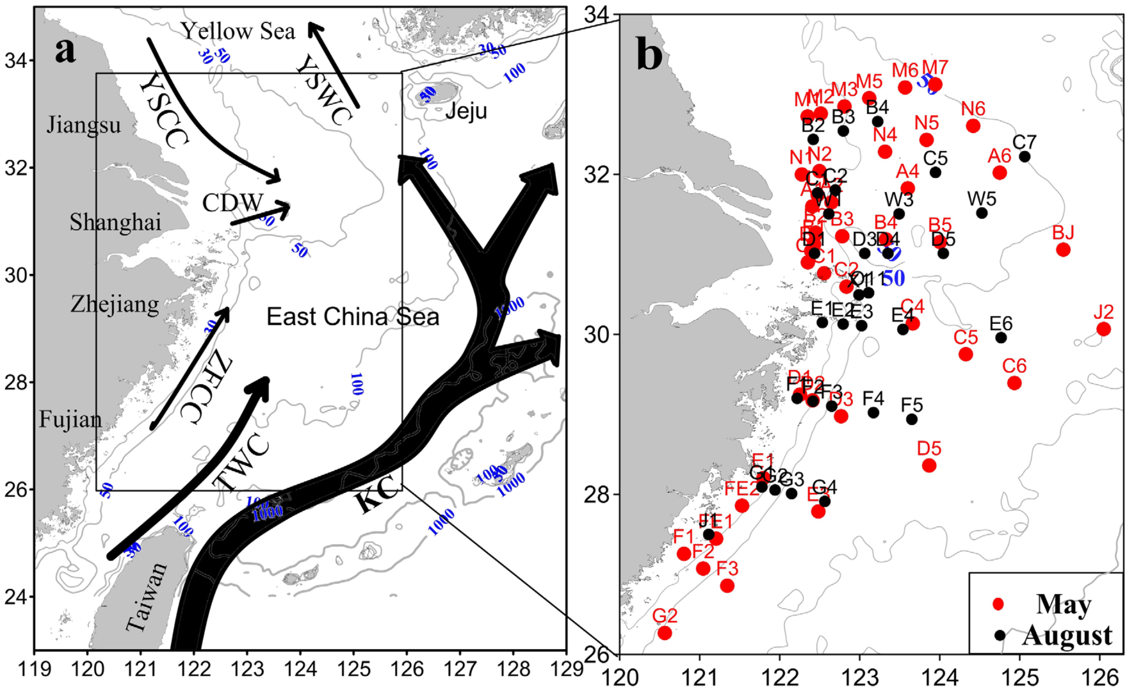


**Figure 1.** (a) The regional surface currents in the summer modified after *Su* [2001]: Changjiang Dilute water (CDW); Zhejiang-Fujian Coast Current (ZFCC); Yellow Sea Coastal Current (YSCC); Yellow Sea Warm Current (YSWC); Taiwan Warm Current (TWC); Kuroshio Current (KC). (b) Location of sites occupied during both the spring and summer cruise tracts. The bathymetry (m) of the ECS shelf is also shown by blue lines.

close to the Changjiang River mouth, in the subaqueous delta: fine sand and silt facies; silty clay, clayey silt facies; sand-silt-clay facies [*Chen et al.*, 2000]. In the waters of the north ECS continental shelf and southwest Jeju Island, there is a fine-grained muddy area surrounded by a sandy deposition area. This mud area is the center of deposition in the northern ECS continental shelf [*Guo et al.*, 2006; *Liu et al.*, 2007].

There are several intricate currents in the ECS, as described in *Su* [2001] (Figure 1a). In the southern portion of the study area, there are two northward currents; one is the warm and salty Kuroshio Current (KC), which flows along the shelf break of the ECS, and the other is the Taiwan Warm Current (TWC). The KC has an average flow ~1000 times higher than that of the Changjiang River runoff. The northern TWC flows along the 50 m isobath and is divided into two branches near the Changjiang River estuary, with one to the northeast and another climbing toward the shore mixed with the Changjiang Diluted Water (CDW), which flows southward in spring and northeastward in summer. Both of these currents mainly dominate the ECS circulation current and significantly influence the distribution of water masses and sedimentation. Near the Changjiang River mouth there is the southeastern Yellow Sea Coastal Current (YSCC) in the north and Zhejiang-Fujian Coastal Current (ZFCC) in the south. There is also a northward Yellow Sea Warm Current (YSWC) parallel to the YSCC. Near the southern Jeju Island, there is a circulation current that is strong in the winter and weak in the summer due to the monsoon climate. The ZFCC flows southward from the Changjiang Delta with a width of about ~30–50 km; the ZFCC has a high flow potential in winter and weak flow potential in summer due to the monsoon climate.

### 2.2. Sampling and Analysis

Sediment samples were collected during the R/V "Shiyan 3" cruise in spring. The sampling lasted for 25 days from 15 May 2011 to 4 June 2011. In summer, the field sampling was conducted on the "Beidou" cruise, which lasted for 10 days, from 16 to 26 August 2011 (Figure 1b) using a box core and subsampled with a 10 cm (diameter) plexiglas core tube. The thickness of the MM was measured from the visual observation of yellowish color in the box core and the clear boundary compared to the underlying layer along with the water content measurements. The MM samples were collected from the cores using a stainless steel knife, put in resealable plastic bags, and then stored at 4°C for subsequent laboratory analyses. Aliquots of these samples were oven dried at 60°C for several days, and the water contents were calculated gravimetrically. The porosity [*Baskaran and Naidu*, 1995] was calculated from the following formula

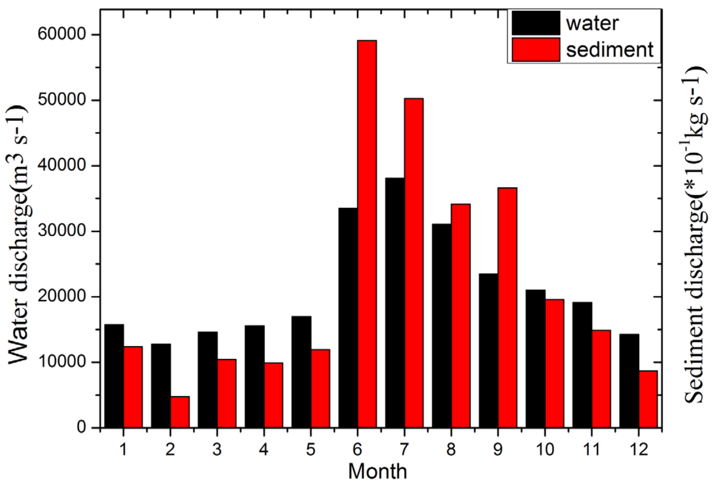


**Figure 2.** Monthly variations of the amounts of water and sediment discharge in 2011 at Datong station of the Changjiang River.

$$\text{Porosity}(\Phi_i)=\frac{f_w}{f_w+(1-f_w)\rho_w/\rho_s}, \quad (1)$$

where $f_w$ is the fractional water content of the MM, $\rho_w$ is the water density (1.025 g cm$^{-3}$), and $\rho_s$ is the dry density of solid particles, assumed to be 2.5 g cm$^{-3}$. The cumulative mass depths ($M$ in g cm$^{-2}$) for the sediment cores were calculated from the following equation

$$M=\sum_i((1-\phi_i)\times\rho_s\times\delta_x), \quad (2)$$

where $\phi_i$ is the porosity of the $i$th section and $\delta_x$ is the thickness of each interval (1 cm).

An aliquot of the wet sample was taken in a beaker, and 5 mL of 5% $H_2O_2$ and 5 mL of 0.2 *M* HCl were added. The organic matter was allowed to oxidize, and the coatings of metal oxides were removed from the mineral grains after ~12–18 h. After that, 10 mL of 0.5 *M* sodium hexametaphosphate solution was added and kept in the ultrasonic bath for 15 min to completely disaggregate the sediment. This solution was used for grain size analysis using a laser particle analyzer (LS100Q, Beckman, USA) and the fractions of clay, silt, and sand were calculated by the mehtod outlined in *Folk and Ward* [1957]. The grain size distribution of the sediments was defined as sand (2000–62.5 $\mu$m), silt (62.5–3.9 $\mu$m), and clay (3.9–0.2 $\mu$m) [*Lane*, 1947]. The slurry was dried in an utility oven at 55°C for ~4 days. The dried sample was homogeneously pulverized, weighed, and then sealed in a plastic box (70 mm diameter × 70 mm height) for radionuclide analysis. The activities of $^{210}Pb_{ex}$, $^{234}Th$, $^{7}Be$, and $^{137}Cs$ in sediment samples were measured following the method described by *Du et al*. [2010]. The radioactivities of the above nuclides were measured using a HPGe $\gamma$ ray detector (Canberra Be3830) with a relative counting efficiency of 35% and an energy resolution of 1.8 keV (at 1332 keV). The detector has multilayer shielding (ultralow cryostat and no peak background in the isotopes of interest). The activities of $^{7}Be$ and $^{137}Cs$ were determined from the $\gamma$ ray peak at 477.6 keV (10.5%) and 661.6 keV (85%), respectively. $^{234}Th$ was determined by using a $\gamma$ ray at 63.3 keV (4.84%) within 3 months of collection and then recounted after 6 months after the decay of excess $^{234}Th$ ($^{234}Th_{ex}$) to quantify the supported $^{234}Th$. The activity of $^{210}Pb_{ex}$ was calculated from the activity of total $^{210}Pb$ (46.5 keV, 4.25%) minus the activity of $^{226}Ra$, determined using the $\gamma$ lines at 351.9 keV (37.6%) for $^{214}Pb$ and 609.3 keV (46.1%) for $^{214}Bi$. To measure the activity of $^{226}Ra$, the samples were sealed for at least 3 weeks to establish a secular equilibrium between $^{226}Ra$ and the daughter products of $^{222}Rn$. The efficiency calibration of the detector systems was conducted using both the Laboratory Sourceless Calibration Software (LabSOCS) and standard samples (GBW04127) to ensure the reliability of the QA/QC method. The data for the nuclides were corrected for the radioactive decay during the time elapsed between sample collection and counting.

## 3. Results

### 3.1. Water and Sediment Discharge of the Changjiang River

The monthly discharges of water and sediment from the Changjiang River to the ECS are given in Figure 2 [*Ministry of Water Resources Changjiang Water Resources Commission*, 2011]. February had the lowest amounts of discharge of both water and sediment, and the highest discharge of sediment occurred in June. There was an overall increasing trend in the water discharge from February to July (Figure 2), along with high wind energy, mainly northerly wind. Between January and May, the dominant winds were from the northwest, controlled by continental weather systems impacting the sedimentation in the Changjiang Delta. In combination with the ZFCC, the CDW moved southward along the shelf to act as the hydrodynamic carrier influencing the inshore MM distribution. The delivery of suspended sediments to the study

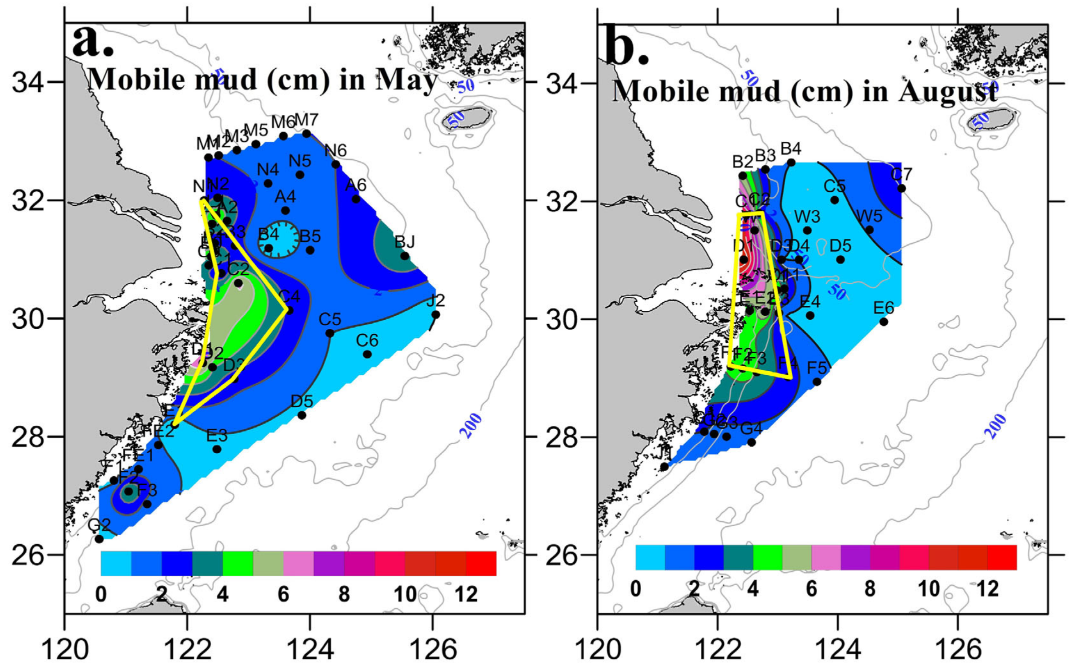


**Figure 3.** Depth of MM (cm) within the confines of our study area (a) from 15 May 2011 to 4 June 2011 and (b) from 16–26 August 2011. The closed areas denote the thick MM layer used to calculate the MM mass.

area is dependent on the amount of river water flow prior to the cruises. According to the report of *Ministry of Water Resources Changjiang Water Resources Commission* [2011], the average runoff in April 2011 had a discharge of more than 15,000 $m^3 s^{-1}$, with even less in the months of March and February, whereas the water discharge during our spring cruise was 17,000 $m^3 s^{-1}$ and gradually increased to 30,000 $m^3 s^{-1}$ by the end of our cruise (Figure 2). Similarly, the sediment discharge in April was also low, below 1000 kg $s^{-1}$, but increased to slightly above 1000 kg $s^{-1}$ during the cruise. However, summer (July–September) was the period of maximum discharge (Figure 2), with high wind energy and occasional typhoons. From July to September, the monsoon marine weather results in southeast wind, making the main branch of the CDW flow toward the northeast and another branch flow toward the southeast. Meanwhile, the water discharge reached the maximum value of 38,000 $m^3 s^{-1}$ ahead of our summer cruise. Although temporal terrestrial sediment deposition (TSD) is high in the Changjiang River mouth during the flood season, total dissolved solids (TDS) would be delivered farther into the ECS by the winter monsoon during the dry season [*Wu et al*., 2013]. In other words, the study area has gone through a period of relatively little sediment delivery to the shelf and relatively weak sediment remobilization during the spring cruise to a period of higher sediment delivery and relatively strong disturbances during the summer cruise.

### 3.2. Distribution Patterns of the MM Thickness

Based on satellite images, it has been reported that the dispersal of Changjiang sedimentary influx in the surface waters forms a turbid plume in the ECS shelf [*Huang et al*., 2013]. Sedimentary particulate matter derived from the Changjiang River has been found over a distance of 250–300 km eastward across the broad shelf. Estimates of the thickness of the MM layer (those sediments that were recently deposited/resuspended) are based on the physical characteristics (color and porosity) documented in the field and laboratory [*Corbett et al*., 2004]. The MM has a yellow, earthy yellow, or gray yellow color, with a porosity ranging between 0.50 and 0.75. The MM thickness in May (Figure 3) varied by over an order of magnitude, from 0.5 to 7.0 cm (average: $2.2 \pm 1.8$ cm). Sediment cores collected along the coast had a MM layer thickness of over 3 cm, and more MM (with a thicker mud layer) was distributed in the south. Most sediment cores collected away from the coast had a MM layer thickness of less than 1 cm, except in the region near station BJ where the thickness was over 3 cm. Similarly, the spatial patterns during the August cruise (Figure 3) showed that the MM thickness ranged from 0.5 to 11 cm (average: $3.9 \pm 3.1$ cm). In contrast to the May cruise, the MM layer had extended farther north in August, especially near the river mouth, with a thickness of 9 cm. The spatial patterns of thickness during both cruise periods showed a clear seasonal variation. The different seasonal distribution in the north of the Changjiang River mouth could have been caused by the delivery of sediments to the study area during the 2 months before the summer cruise. Similarly, MM collected in both cruises was mainly distributed along the coast, and we could use the thickness and density to spatially estimate the mass. The area of MM along the coast in the spring and summer cruises was estimated to be 21,600 and 15,000 km$^2$, respectively, using Google Earth, shown as the closed area in Figure 3. The average thicknesses were $3.0 \pm 2.0$ and $4.8 \pm 3.0$ cm in spring and summer, respectively. Considering a MM bulk density of 1.2 g cm$^{-3}$, the estimated mass of MM is $(7.8 \pm 5.1) \times 10^8$ and $(8.8 \pm 5.4) \times 10^8$ t in May and August, respectively. The MM covered a larger area in May but with less mass compared to August. The MM mass is 4 times larger than the annual Changjiang sediment discharge of $2 \times 10^8$ t yr$^{-1}$. The tide and current around this area could be the major factor for the formation and maintenance of MM in the southern coastal belt.

### 3.3. Grain Size Distribution and Mineral Components of MM

The grain size of MM is listed in Table 1 and plotted in Figure 4. The grain size of MM were 6–49 $\mu$m (mean: 17 $\mu$m) and 5–36 (mean: 15 $\mu$m) in May and August, respectively. Both the average and maximum values of the MM grain size in May appear to be slightly higher than those in August, although one could argue that they are the same within the errors associated with the estimates ($p > 0.05$). The mean grain size distribution of MM in the ECS continental shelf exhibited "fine-coarse-fine" features, indicating the transportation of MM toward the east. The MM in the coastal region is the finest (mean: $<20$ $\mu$m), whereas it is coarser (mean: $>40$ $\mu$m), in the middle part of the shelf; part of this difference is due to the relict sediment deposition during the low sea level in the late Pleistocene [*Chert et al.*, 1985; *Chen et al.*, 2000]. In May, 100 km wide clay and silt MM was found to be uniformly distributed along the south of the Changjiang River estuary coast. The grain size decreased from the Changjiang Delta toward the southeast. The north offshore MM is relatively fine compared to that in the south, in contrast to what was found in August. This observation could be related to the smaller area considered in August.

The mineral components of MM in the north offshore were complex, composed of clay (13%–26%), silt (26%–46%), and sand (27%–58%) (mean grain size: 22–49 $\mu$m). A slightly different grain size variation was observed in the north coast in the grain size distribution of the MM, with a larger mean grain size in May (11–39 $\mu$m, with 13%–24% clay, 37%–67% silt, and 9%–50% sand), with a unimodal frequency percentage and $\Phi$ values of 1–4 (Figure 4a), whereas smaller mean grain sizes (9–34 $\mu$m, with 17%–27% clay, 32%–71% silt and 2.8%–51% sand) were observed in August. The MM along the south coast had a depth of $>2$ cm in both August and May, with $>30\%$ clay, $>63\%$ silt, and $<5\%$ sand. The frequency percentage curve was wide and flat, with a mean grain size of $<9$ $\mu$m (Figure 4b). However, some stations close to the Changjiang River mouth contained $<24\%$ clay and $>10\%$ sand, caused by the strong dynamic river conditions. In the north offshore, the grain size decreased from north to south, with increases in the fine part of double-peak structure (Figures 4c and 4d), indicating fresh material input. The porosity of MM was high along the coast (0.50–0.75), except for several stations in the offshore, where it is relatively low ($<0.50$), likely due to the impact of the coastal current on the granulometric parameters. In summary, the MMs were mainly composed of fine grains, with 85%–99% clay + silt (except for some in the offshore) and a relatively high porosity $>0.50$.

### 3.4. Spatial Distribution of the Activities of $^{7}$Be, $^{234}$Th$_{ex}$, $^{210}$Pb$_{ex}$, and $^{137}$Cs in the MM

The spatial distribution of the activities (Bq kg$^{-1}$) were similar to the inventory distribution patterns, which are discussed below and shown in supporting information Table S1 and Figure S1. The range of $^{7}$Be activities in May and August were not significantly different from each other ($p > 0.05$), varing from 5.1 to 17.6 (mean: $8.6 \pm 3.3$ Bq kg$^{-1}$) and from 5.9 to 8.3 Bq kg$^{-1}$ (mean: $7.0 \pm 1.0$ Bq kg$^{-1}$), respectively. $^{7}$Be is derived primarily from direct atmospheric deposition, which depends on the amount of precipitation and secondarily from watershed erosional input; hence, the activities in shallow water sediments vary seasonally due to changes in the amount of precipitation. Atmospheric fluxes of $^{7}$Be collected over 8 years in Shanghai, China indicate that the highest seasonal atmospheric fluxes occurred during the spring months 75% of the time [*Du et al.*, 2015]. In May, the region south of the Changjiang River had higher $^{7}$Be activities, with a decreasing trend from the river mouth to station F3. In August, the $^{7}$Be distribution coincided with the Changjiang River plume in the summer and decreased toward the northeast. Similarly, the ranges in $^{234}$Th$_{ex}$ activities in both May and August were not significantly different; May: 7–162 Bq kg$^{-1}$ (mean: $85 \pm 54$ Bq kg$^{-1}$); August:

**Table 1.** Geochemical Properties of MM in the ECS

| Sampling Location | Sampling Time | Water Depth (m) | Longitude | Latitude | Thickness (cm) | Mean Grain Size ($\mu$m) | Clay (%) | Silt (%) | Sand (%) | Density (g cm$^{-3}$) | Water | Porosity |
|---|---|---|---|---|---|---|---|---|---|---|---|---|
| G2 | 15 May | 67.0 | 120.57 | 26.27 | 0.5 | 8 | 29.0 | 67.4 | 3.6 | 1.06 | 0.55 | 0.75 |
| F3 | 17 May | 70.0 | 121.35 | 26.86 | 1.5 | 9 | 26.0 | 69.5 | 4.4 | 0.78 | 0.42 | 0.64 |
| F1 | 17 May | 25.1 | 120.81 | 27.26 | 0.5 | 6 | 35.6 | 64.3 | 0.1 | 1.17 | 0.45 | 0.67 |
| FE1 | 17 May | 30.0 | 121.21 | 27.45 | 1.5 | 6 | 33.3 | 65.6 | 1.1 | 1.09 | 0.43 | 0.65 |
| FE2 | 17 May | 29.0 | 121.53 | 27.86 | 1.1 | 6 | 36.2 | 63.5 | 0.3 | 1.18 | 0.47 | 0.69 |
| E1 | 18 May | 23.0 | 121.80 | 28.21 | 0.5 | 6 | 33.9 | 65.7 | 0.5 | 1.04 | 0.50 | 0.72 |
| D3 | 21 May | 62.8 | 122.77 | 28.98 | 2.5 | 8 | 33.9 | 51.8 | 14.2 | 1.16 | 0.53 | 0.74 |
| D1 | 21 May | 17.0 | 122.25 | 29.25 | 7.0 | 7 | 31.5 | 67.8 | 0.7 | 1.20 | 0.47 | 0.69 |
| C2 | 22 May | 40.0 | 122.83 | 30.60 | 6.5 | 7 | 32.6 | 66.0 | 1.4 | 1.26 | 0.46 | 0.68 |
| C4 | 22 May | 67.4 | 123.66 | 30.14 | 1.0 | 20 | 25.6 | 32.0 | 42.5 | 1.27 | 0.34 | 0.56 |
| C5 | 22 May | 76.2 | 124.33 | 29.75 | 1.0 | 26 | 24.0 | 30.4 | 45.6 | 1.30 | 0.16 | 0.33 |
| BJ | 24 May | 64.9 | 125.55 | 31.06 | 3.6 | 15 | 26.0 | 46.6 | 27.5 | 1.23 | 0.47 | 0.69 |
| B3 | 25 May | 49.7 | 122.78 | 31.23 | 2.5 | 49 | 15.8 | 25.9 | 58.3 | 1.27 | 0.31 | 0.52 |
| B2 | 25 May | 20.0 | 122.45 | 31.27 | 2.0 | 11 | 24.2 | 66.5 | 9.3 | 1.17 | 0.23 | 0.42 |
| N6 | 26 May | 49.0 | 124.42 | 32.61 | 2.0 | 41 | 17.5 | 28.7 | 53.8 | 1.33 | 0.20 | 0.39 |
| N1 | 27 May | 20.6 | 122.28 | 32.00 | 2.5 | 25 | 15.1 | 53.5 | 31.4 | 1.44 | 0.31 | 0.53 |
| M2 | 27 May | 27.9 | 122.51 | 32.76 | 0.7 | 39 | 13.3 | 37.2 | 49.5 | 1.32 | 0.25 | 0.45 |
| M3 | 27 May | 32.0 | 122.81 | 32.85 | 1.0 | 46 | 13.7 | 30.5 | 55.8 | 1.37 | 0.25 | 0.45 |
| M5 | 27 May | 35.7 | 123.12 | 32.95 | 1.5 | 31 | 18.4 | 36.3 | 45.4 | 1.25 | 0.26 | 0.46 |
| M6 | 27 May | 38.6 | 123.57 | 33.09 | 2.0 | 6 | 34.1 | 63.2 | 2.6 | 1.24 | 0.44 | 0.66 |
| M7 | 27 May | 56.1 | 123.95 | 33.13 | 2.0 | 37 | 18.8 | 28.3 | 52.9 | 1.28 | 0.41 | 0.64 |
| L1 | 1 Jul | 26.0 | 122.47 | 31.74 | 5.0 | 16 | 18.8 | 66.2 | 15.0 | 1.28 | 0.37 | 0.59 |
| B1 | 1 Jul | 14.0 | 122.43 | 31.13 | 5.0 | 7 | 30.5 | 66.5 | 3.0 | 1.37 | 0.42 | 0.65 |
| B0 | 2 Jul | 13.0 | 122.39 | 31.04 | 0.5 | 6 | 33.9 | 65.5 | 0.7 | 1.08 | 0.37 | 0.59 |
| C0 | 2 Jul | 15.0 | 122.35 | 30.90 | 1.0 | 7 | 30.7 | 67.6 | 1.7 | 1.17 | 0.29 | 0.50 |
| C1 | 2 Jul | 19.0 | 122.56 | 30.77 | 1.5 | 8 | 28.0 | 67.9 | 4.1 | 1.29 | 0.40 | 0.62 |
| D2 | 2 Jul | 39.0 | 122.41 | 29.18 | 4.0 | 5 | 36.8 | 63.1 | 0.1 | 1.11 | 0.54 | 0.74 |
| F2 | 4 Jul | 46.1 | 121.04 | 27.08 | 4.5 | 6 | 33.3 | 66.0 | 0.8 | 1.15 | 0.42 | 0.64 |
| 8J1 | 16 Aug | 27.3 | 121.11 | 27.50 | 1.0 | 5 | 37.7 | 62.3 | 0.0 | 1.07 | 0.55 | 0.76 |
| 8G1 | 17 Aug | 24.7 | 121.78 | 28.10 | 2.0 | 5 | 37.1 | 62.5 | 0.5 | 1.07 | 0.48 | 0.70 |
| 8G2 | 17 Aug | 43.2 | 121.94 | 28.06 | 1.5 | 7 | 32.0 | 67.5 | 0.5 | 1.15 | 0.44 | 0.66 |
| 8F4 | 19 Aug | 72.4 | 123.17 | 29.02 | 2.5 | 7 | 38.9 | 51.2 | 9.9 | 1.16 | 0.49 | 0.70 |
| 8F3 | 19 Aug | 54.0 | 122.65 | 29.10 | 4.0 | 10 | 21.9 | 75.4 | 2.7 | 1.10 | 0.48 | 0.70 |
| 8F2 | 19 Aug | 33.3 | 122.42 | 29.17 | 5.0 | 6 | 34.5 | 65.4 | 0.1 | 1.15 | 0.49 | 0.70 |
| 8F1 | 19 Aug | 17.8 | 122.22 | 29.20 | 4.0 | 8 | 26.9 | 71.9 | 1.2 | 1.06 | 0.40 | 0.62 |
| 8E1 | 20 Aug | 22.0 | 122.53 | 30.15 | 3.5 | 6 | 32.1 | 67.2 | 0.7 | 1.09 | 0.50 | 0.71 |
| 8E2 | 20 Aug | 42.0 | 122.79 | 30.13 | 7.0 | 6 | 32.9 | 66.0 | 1.1 | 1.13 | 0.44 | 0.66 |
| 8E3 | 20 Aug | 48.0 | 123.02 | 30.11 | 1.0 | 36 | 18.1 | 31.6 | 50.2 | 1.23 | 0.39 | 0.61 |
| 8X1 | 21 Aug | 57.0 | 122.99 | 30.49 | 5.0 | 20 | 22.3 | 44.4 | 33.3 | 1.24 | 0.43 | 0.65 |
| 8D1 | 21 Aug | 17 | 122.44 | 31.01 | 11.0 | 5 | 39.5 | 60.2 | 0.3 | 1.20 | 0.43 | 0.65 |
| 8C1 | 24 Aug | 26.0 | 122.47 | 31.77 | 11.0 | 9 | 25.9 | 71.3 | 2.8 | 1.18 | 0.47 | 0.69 |
| 8C2 | 24 Aug | 34.1 | 122.69 | 31.80 | 2.5 | 22 | 20.6 | 43.9 | 35.5 | 1.22 | 0.45 | 0.67 |
| 8C7 | 25 Aug | 50.4 | 125.06 | 32.22 | 3.0 | 44 | 15.5 | 28.9 | 55.6 | 1.21 | 0.41 | 0.63 |
| 8B4 | 26 Aug | 36.2 | 123.22 | 32.66 | 1.0 | 26 | 18.6 | 43.0 | 38.3 | 1.22 | 0.43 | 0.65 |
| 8B3 | 26 Aug | 34.2 | 122.80 | 32.54 | 2.0 | 34 | 16.8 | 32.3 | 50.9 | 1.17 | 0.40 | 0.62 |

6–168 Bq kg$^{-1}$ (mean: 44 $\pm$ 7 Bq kg$^{-1}$). In contrast to the distribution of $^{7}$Be, $^{234}$Th$_{ex}$ was found to be below detection limit (BDL) in the northern region in both May and August. The distribution of $^{234}$Th$_{ex}$ during these 2 months exhibited similar patterns, with higher values found south of the Hangzhou Bay and a decreasing trend from south to north and from offshore to coast.

The $^{137}$Cs activities in May and August ranged between 0.8 and 3.5 Bq kg$^{-1}$ (mean: 2.0 $\pm$ 0.7 Bq kg$^{-1}$) and between 1.0 and 3.1 Bq kg$^{-1}$ (mean: 1.7 $\pm$ 0.6 Bq kg$^{-1}$), respectively. Moreover, the activities of $^{137}$Cs in May decreased from the coast to offshore, with a maximum value near the river mouth. In contrast, the maximum activities in August were found in the southern region, possibly indicating another source of $^{137}$Cs. The $^{210}$Pb$_{ex}$ activities in the MM in May and August ranged between 5.3 and 171 (mean: 59 $\pm$ 36 Bq kg$^{-1}$) and between 5.4 and 150 Bq kg$^{-1}$ (mean: 63 $\pm$ 41 Bq kg$^{-1}$), respectively. A decreasing trend of $^{210}$Pb$_{ex}$ activity was observed from the coast to offshore in May but not in August. The $^{210}$Pb$_{ex}$ activities in the south of the study area were higher than those in the north during both cruises. In the north inshore, the $^{210}$Pb$_{ex}$ activities were higher in August than in May, and the MM in the south inshore showed similar pattern.

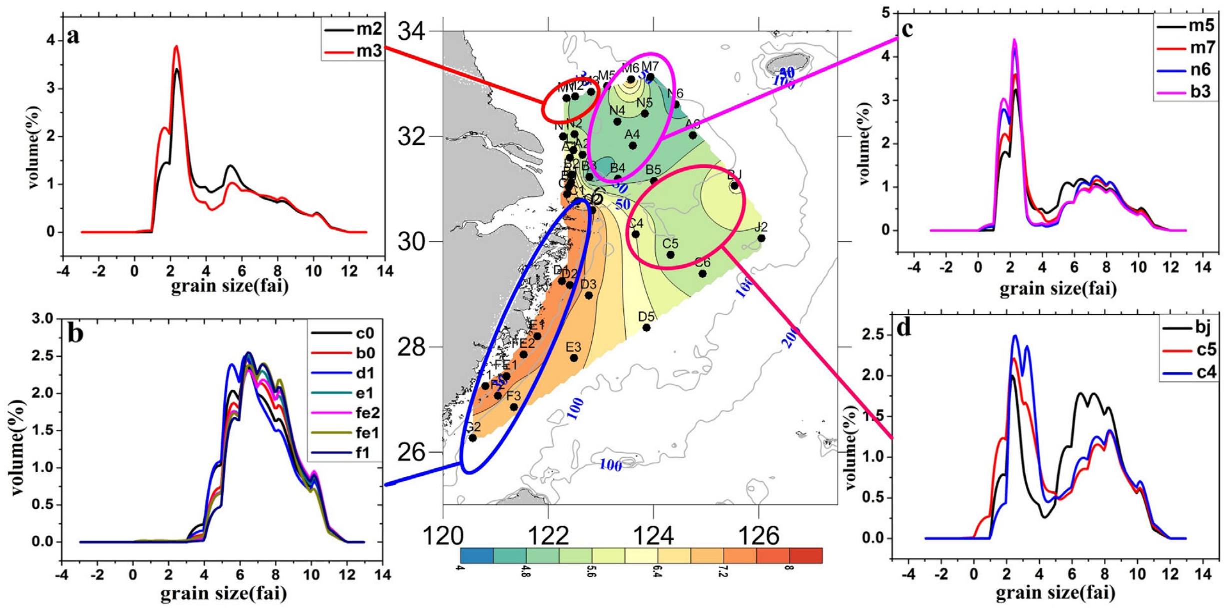


**Figure 4.** Grain size frequency percentage distribution of the MM.

## 4. Discussion

### 4.1. MM Features in the ECS

The delivery of river-borne sediments into the coastal areas through the estuary is greatly influenced by the temporary storage and remobilization of MM [*McKee and Baskaran*, 1999; *Corbett et al*., 2004]. The thickness and spatial distribution of MM in the two seasons adjacent to the river vary seasonally, similar to findings in the Mississippi River deltaic region [*Corbett et al*., 2004]. The porosity of the MM layer in all cores decreased from the top layer until reaching a constant value, with no change in the MM layer color (Figure 5). MM can affect the biogeochemical processes significantly with the formation of oxidation and cyclical reduction during early diagenesis in the sediments [*Aller et al*., 2004; *Corbett et al*., 2004] and makes Fe and Mn undergo reexposure and reoxidation repeatedly to accelerate the oxygen-consuming process [*Aller et al*., 2004], which may lead to MM with a yellowish color. No macrofauna and shell particles were observed in MM at the time of sample collection, except in a few cores with the thin MM layer. Thus, bioturbation does not appear to be an important mixing process in forming the MM layer in the region where the MM depth is thick; however, physical mixing homogenizes the MM layer. The mean thickness of the MM in May (2.2 cm: range: 0.5–7.0 cm) and August (3.9 cm; range: 0.5–11.0 cm) is comparable to the thickness of $<$3 cm away from the major influence of the Mississippi River to 12 cm closer to the Southwest Pass near the Mississippi River mouth [*Corbett et al*., 2004] but are considerably lower than the values of 50–200 cm in the Amazon River mouth and 30–100 cm in the Papua Gulf [*Aller et al*., 2004; *Bianchi et al*., 2007]. The mean grain size of MM remained constant in the general surface sediments, including its clay and silt components (Table 2). The water content (porosity) of MM is higher than that of general surface sediments, and this difference is often used to distinguish these two types of sediments.

### 4.2. Vertical Profiles and Inventories of $^{7}$Be, $^{234}$Th$_{ex}$, $^{210}$Pb$_{ex}$, and $^{137}$Cs in the MM

The inventories of $^{137}$Cs and $^{210}$Pb$_{ex}$ in the sediment cores (Figure 6 and Table 2) obtained by integrating its activity at the measured layers and interpolating in-between layers yielded values of 512, 371, 1517, and 877 Bq m$^{-2}$ and 13.8, 7.4, 22.1, and 16.3 kBq m$^{-2}$ at 8C1, 8E2, D2, and BJ, respectively. The inventory of $^{137}$Cs and $^{210}$Pb$_{ex}$ in May are significantly higher than those in August at the south inshore (D2 $>$ 8E2), likely due to the southward transportation of sedimentary material by the CDW and ZFCC in spring. The inventory of $^{137}$Cs and $^{210}$Pb$_{ex}$ at the river mouth (8C1) are significantly higher than those in the south (8E2), suggesting that the northeastward CDW likely transported and deposited material in the northern part. There is no gradient in the activities of $^{137}$Cs and $^{210}$Pb$_{ex}$ in the three coastal cores, indicating homogenous mixing within the MM, and thus the sedimentation rate within MM cannot be estimated. Station BJ site had large

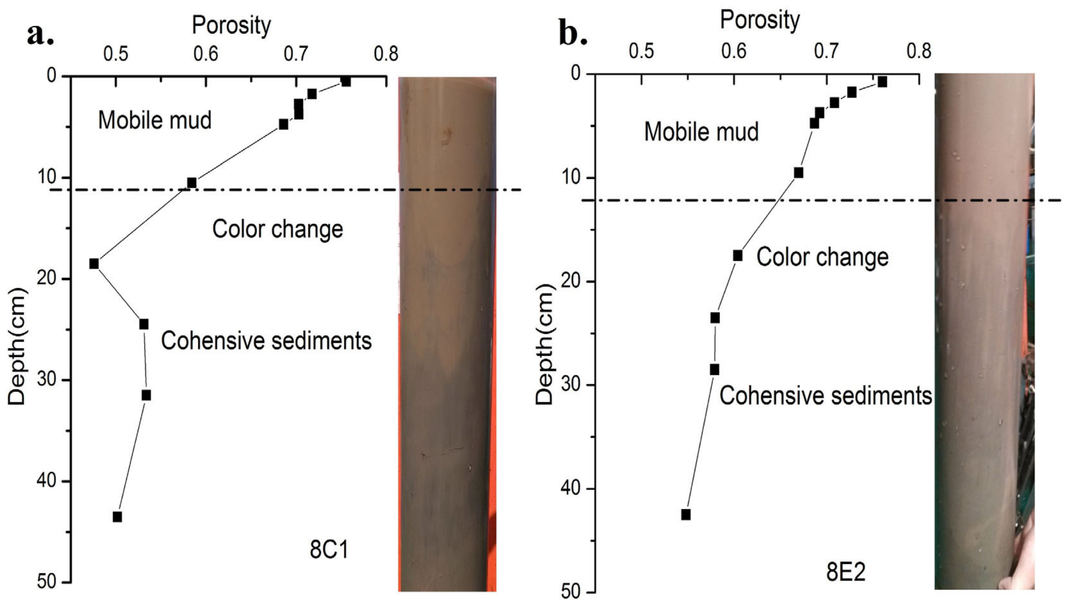


**Figure 5.** Changes in the porosity values and colors change of two typical cores collected from the north coast (Site 8C1) and south coast (8E2) environments during the summer cruise.

inventories of $^{137}Cs$ and $^{210}Pb_{ex}$, even higher than those in the river mouth (8C1), suggesting that there is a large influx of these nuclides to this region. The sedimentation rate calculated by $^{210}Pb_{ex}$ is 0.9 cm yr$^{-1}$, providing further support for additional sediment input and deposition.

The MM inventory ($I_x$, where $x$ is the radionuclide) is calculated as follows

$$I_x(\mathrm{Bq\ m^{-2}}) = A_x \times \rho_b \times d, \tag{3}$$

where $A_x$ is the activity of the nuclide (Bq kg$^{-1}$, $^{7}Be$, $^{234}Th_{ex}$, $^{210}Pb_{ex}$, or $^{137}Cs$), $\rho_b$ is the bulk density (kg m$^{-3}$), and $d$ is the thickness of the MM (in m). As presented earlier, $^{7}Be$ does not have any detectable in situ production source, and hence the supply of $^{7}Be$ to shelf sediments is primarily controlled by atmospheric deposition. The $^{7}Be$ inventory (Figures 7a and 7e) in MM is similar to the average atmospheric depositional flux of $^{7}Be$ during 8 years in Shanghai, China (309 Bq m$^{-2}$). This flux was obtained by using the $^{7}Be$ deposition flux in Shanghai (1467 Bq m$^{-2}$ yr$^{-1}$) [*Du et al.*, 2015] multiplied by the mean-lifetime of $^{7}Be$ (0.21 year). The inventories of $^{7}Be$ in MM varied between the BDL to 513 Bq m$^{-2}$. The higher values were found south of the study area in May and north of the study area in August, reflecting a similar variation pattern as the CDW. The ratio of the measured $^{7}Be$ inventory to that of the atmospheric depositional flux decreased from inshore to offshore, except at 8C7 (0.8). Larger ratios (in N1, C2, D2, and 8X1 $\geq$ 1) were found along the coast, suggesting that the riverine contribution was significant. The Changjiang plume branch in summer ends at 33.5°N [*Wu et al.*, 2014], and Changjiang riverine materials can be transported to this area [*Lim et al.*, 2006; *Wang et al.*, 2009]; thus the high ratio of $^{7}Be$ in 8C7 during August is likely due to the Changjiang River input. In summary, the $^{7}Be$ distribution reflected the seasonal variations of materials by atmospheric deposition and riverine input, as reflected in the higher precipitation amounts, leading to a larger amount of discharge and atmospheric fallout.

The inventories of $^{234}Th_{ex}$ (Figures 7b and 7f) in May and August were not significantly different and varied from BDL to 5638 and from BDL to 4869 Bq m$^{-2}$, respectively. The spatial distribution showed several high value centers in both seasons and generally decreased from offshore to inshore. We can evaluate accelerated sediment deposition and/or sediment focusing using the ratio of measured excess $^{234}Th$ to the water column-supported $^{234}Th$ inventory. The surface and bottom water salinities in the ECS ranged from ~23 to 34 and from ~29 to 34, respectively (supporting information Table S2), and the residence times of $^{234}Th_{ex}$ in the water column of the ECS ranged from 0.18 to 4.1 days [*Huang et al.*, 2010]. Thus, the water-column-supported $^{234}Th$ ($W$, Bq m$^{-2}$), following complete scavenging and one-dimensional vertical flux, can be calculated by integrating the production of $^{234}Th$ at different water column depths (m) and calculating the activity of $^{238}U$ from the $^{238}U$-salinity relationship [*Corbett et al.*, 2004; *Huang et al.*, 2013].

**Table 2.** Inventories of $^{210}$Pbex and $^{137}$Cs in Sediment Cores From the ECS[a]

| Sample | Mean Grain Size ($\mu$m) | Water Content | Porosity | Mass Depth (g cm$^{-2}$) | $^{137}$Cs (mBq cm$^{-2}$) | $^{210}$Pb$_{ex}$ (mBq cm$^{-2}$) |
|---|---|---|---|---|---|---|
| *8C1 (122.35°E, 30.90°N, 13 m Depth)* | | | | | | |
| 0–1 | 11.94 | 0.55 | 0.76 | 0.5 | LD | 22.56 ± 6.69 |
| 1.5–2 | 10.81 | 0.50 | 0.72 | 1.75 | LD | 31.91 ± 8.19 |
| 2.5–3 | 12.04 | 0.49 | 0.70 | 2.75 | LD | 35.68 ± 8.44 |
| 3.5–4 | 10.90 | 0.49 | 0.70 | 3.75 | LD | 36.99 ± 8.02 |
| 4.5–5 | 11.83 | 0.47 | 0.69 | 4.75 | LD | 30.18 ± 8.70 |
| 10–11 | 16.75 | 0.36 | 0.58 | 10.5 | 1.41 ± 0.55 | 33.48 ± 8.75 |
| 18–19 | 24.46 | 0.27 | 0.48 | 18.5 | LD | 28.76 ± 8.65 |
| 24–25 | 28.25 | 0.31 | 0.53 | 24.5 | LD | 14.85 ± 8.71 |
| 31–32 | 21.28 | 0.31 | 0.53 | 31.5 | 1.91 ± 0.81 | 18.79 ± 9.64 |
| 43–44 | 18.56 | 0.29 | 0.50 | 43.5 | 2.33 ± 0.91 | 39.52 ± 11.17 |
| *8E1 (122.5°E, 30.15°N, 22 m Depth)* | | | | | | |
| 0.5–1 | 7.20 | 0.56 | 0.76 | 0.75 | LD | 13.28 ± 3.67 |
| 1.5–2 | 6.54 | 0.52 | 0.73 | 1.75 | LD | 18.14 ± 4.44 |
| 2.5–3 | 7.41 | 0.49 | 0.71 | 2.75 | LD | 16.87 ± 4.34 |
| 3.5–4 | 7.72 | 0.47 | 0.69 | 3.75 | LD | 16.52 ± 4.38 |
| 4.5–5 | 7.38 | 0.47 | 0.69 | 4.75 | 0.75 ± 0.36 | 16.48 ± 4.27 |
| 9–10 | 8.41 | 0.45 | 0.67 | 9.5 | 1.52 ± 0.39 | 27.54 ± 6.21 |
| 17–18 | 7.93 | 0.38 | 0.60 | 17.5 | 1.44 ± 0.63 | 14.22 ± 8.17 |
| 23–24 | 7.85 | 0.36 | 0.58 | 23.5 | 1.29 ± 0.49 | 12.99 ± 5.89 |
| 28–29 | 7.95 | 0.35 | 0.58 | 28.5 | LD | 18.93 ± 8.74 |
| 42–43 | 8.00 | 0.33 | 0.55 | 42.5 | LD | 18.12 ± 8.99 |
| *D2 (122.41°E, 29.18°N, 39 m Depth)* | | | | | | |
| 0.5–1 | 8.11 | 0.52 | 0.73 | 0.75 | LD | 75.17 ± 12.27 |
| 1.5–2 | 8.61 | 0.47 | 0.69 | 1.75 | LD | 51.87 ± 7.95 |
| 2.5–3 | 7.18 | 0.49 | 0.71 | 2.75 | 2.96 ± 1.23 | 53.76 ± 6.51 |
| 3.5–4 | 7.60 | 0.43 | 0.66 | 3.75 | LD | 41.95 ± 7.77 |
| 4.5–5 | 8.03 | 0.53 | 0.74 | 4.75 | LD | 42.28 ± 7.99 |
| 10–11 | 8.61 | 0.40 | 0.62 | 10.5 | 5.15 ± 1.04 | 56.14 ± 7.77 |
| 18–19 | 8.04 | 0.38 | 0.61 | 18.5 | 2.25 ± 1.25 | 63.92 ± 7.61 |
| 24–25 | 8.87 | 0.35 | 0.57 | 24.5 | 3.97 ± 1.10 | 49.33 ± 6.73 |
| 29–30 | 6.86 | 0.40 | 0.62 | 29.5 | 4.13 ± 1.00 | 56.59 ± 6.19 |
| 36–37 | 7.51 | 0.38 | 0.60 | 36.5 | 6.36 ± 1.04 | 37.20 ± 6.22 |
| 42–43 | 12.57 | 0.33 | 0.55 | 42.5 | 4.05 ± 1.63 | 55.77 ± 9.34 |
| *BJ (125.55°E, 31.06°N, 65 m Depth)* | | | | | | |
| 0–1 | 7.77 | 0.52 | 0.73 | 1.75 | LD | 54.87 ± 9.57 |
| 1.5–2 | 9.46 | 0.42 | 0.65 | 2.75 | 1.75 ± 1.28 | 62.42 ± 7.36 |
| 2.5–3 | 21.15 | 0.39 | 0.62 | 3.75 | LD | 42.30 ± 7.78 |
| 3.5–4 | 12.73 | 0.37 | 0.60 | 4.75 | 3.85 ± 1.49 | 33.44 ± 7.92 |
| 4.5–5 | 9.47 | 0.39 | 0.61 | 10.5 | 1.58 ± 1.34 | 44.78 ± 6.17 |
| 10–11 | 10.06 | 0.35 | 0.57 | 17.5 | 1.57 ± 0.94 | 54.98 ± 5.81 |
| 17–18 | 10.46 | 0.35 | 0.58 | 25.5 | 4.30 ± 1.24 | 56.51 ± 8.99 |
| 25–26 | 7.14 | 0.37 | 0.60 | 32.5 | 1.96 ± 0.92 | 34.03 ± 4.70 |
| 32–33 | 9.91 | 0.37 | 0.60 | 37.5 | 2.47 ± 1.54 | 24.13 ± 6.90 |
| 37–38 | 8.66 | 0.40 | 0.62 | 43.5 | 1.82 ± 1.14 | 22.58 ± 2.94 |

[a]LD: lower than detection limit.

$$A_n=0.983\times S_n+4.3, \tag{4}$$

$$W=\sum_{0}^{N}(n\times A_n), \tag{5}$$

where $S_n$ is the salinity (psu) of seawater with water depth $n$ (m) and $A_n$ is the $^{238}$U activity (Bq m$^{-3}$). The original data are given in supporting information Table S2. The ratios of greater than 1 indicates area of sediment focusing or accelerated mass accumulation. Regions with higher ratios (Figures 8a and 8b) were found in the south inshore (>2.5) during both cruises, with notable sediment focusing associated with the ZFCC and TWC during May. Taking a water depth of 50 m in the north offshore, the large ratio in this area indicates that the increased mass flux may have been associated with the circulation current.

The $^{210}$Pb$_{ex}$ inventory in MM (Figures 7d and 7h) varied between 126 and 5468 Bq m$^{-2}$, with the maximum values found closer to the river mouth in May and closer to the south offshore in August. In May, the inventories of $^{210}$Pb$_{ex}$ decreased from the river mouth to offshore, indicating the transport of river-borne material.

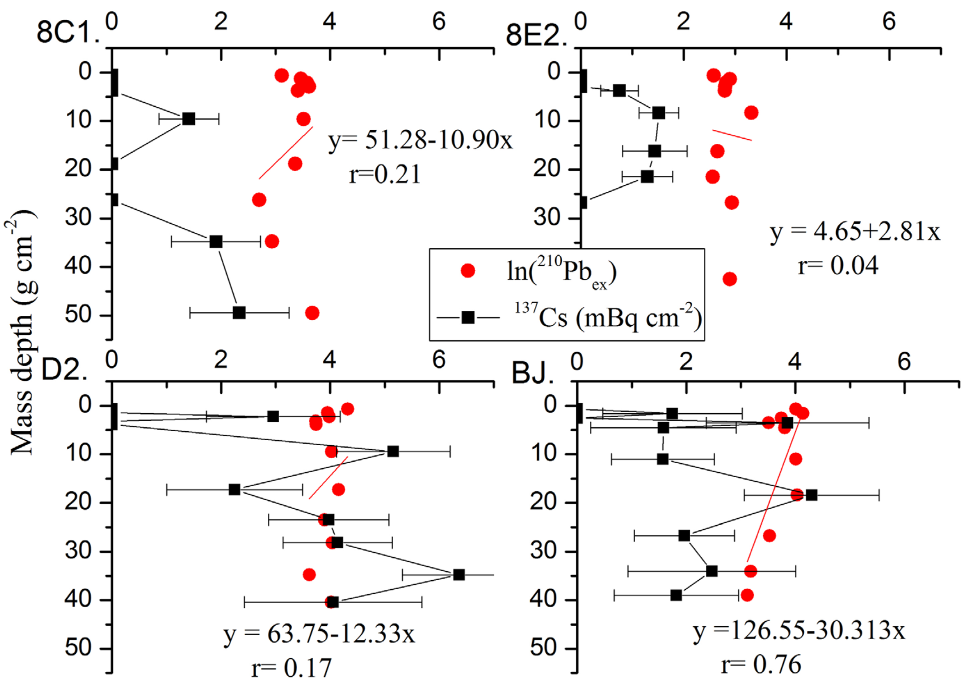


**Figure 6.** Vertical distribution of $^{137}Cs$ (mBq cm$^{-2}$) and ln ($^{210}Pb_{ex}$) in four cores: 8C1 was collected in the north inshore, D2 and 8E2 were collected in the south inshore, and BJ was collected in the north open shelf.

In August, the $^{210}Pb_{ex}$ inventories decreased from south offshore to inshore, which may be related to the higher nutrient flux from offshore upwelling, which in turn will result in an enhanced scavenging process [*Liu et al*., 2006]. The inventory of $^{137}Cs$ in MM varied between BDL to 238 Bq m$^{-2}$, with the highest values found closer to the river mouth where the Changjiang River-derived particulate matter dominate (Figures 7c and 7g). The spatial distribution of $^{137}Cs$ inventories in the two seasons showed highly similar patterns.

### 4.3. Residence Time of the MM

One can estimate the residence time of MM using a simple box-model approach. The sources of MM to the box include riverine contribution and resuspended mud within the box. At the steady state, the mass coming into the box equals the mass exiting the box. If the advectional input into the box equals the advectional output, and sediment long-term burial is the only mechanism of removal, then the residence time of MM ($\tau_{mm}$) is given by

$$\tau_{mm} = I_{mm}/I_{ri}, \tag{6}$$

where the $I_{mm}$ is the inventory of MM (ton) in the box and $I_{ri}$ is the annual riverine input of <63 $\mu$m sediments in the study area (2 $\times$ 10$^8$ t yr$^{-1}$). The sediment discharged by the Yellow Sea had a weak influence on the mass balance of sediment in the south coastal area (closed area in Figure 3) [*Liu et al*., 2007]; thus, this simple approach involves that all of the sediments discharged by the Changjiang River are found within the box and that the net sediments coming into the box from other sources is negligible (total nonriverine MM coming in = MM going out). It is assumed that the MM continues to recycling a number of times before its eventual burial. Equation (7) yields a residence time of ~4 ± 2 years, based on several simple assumptions regarding advectional transport and the amount of MM coming from the Changjiang River. This estimate can also be compared to the residence time obtained from a comparison of the inventories of $^{210}Pb$ in the MM to that of the annual atmospheric fallout and riverine input. Taking the total mass of MM as (7.8 ± 5.1) $\times$ 10$^8$ t (May) and (8.8 ± 5.4) $\times$ 10$^8$ t (August), and the average activity of MM as 44 ± 27 Bq/kg in May and 50 ± 38 Bq/kg in August, respectively, we obtain an inventory of 1589 ± 1414 Bq m$^{-2}$ for May and 2933 ± 2845 Bq m$^{-2}$ for August for a total surface area of 2.16 $\times$ 10$^{10}$ m$^2$ (May) and 1.5 $\times$ 10$^{10}$ m$^2$ (August). The average annual atmospheric fallout in Shanghai, the nearest city where we have long-term atmospheric fallout data, is 366 Bq m$^{-2}$ yr$^{-1}$ [*Du et al*., 2015]. *Su and Huh* [2002] and *Du et al*. [2010] reported that atmospheric fallout and riverine input are the main sources of $^{210}Pb$ in this closed area (Figure 3), and the Changjiang riverine flux was 115 Bq m$^{-2}$ yr$^{-1}$ [*Su and Huh*, 2002]. From the inventory of $^{210}Pb_{ex}$ in MM and the total annual fallout and riverine input $^{210}Pb$, we obtain

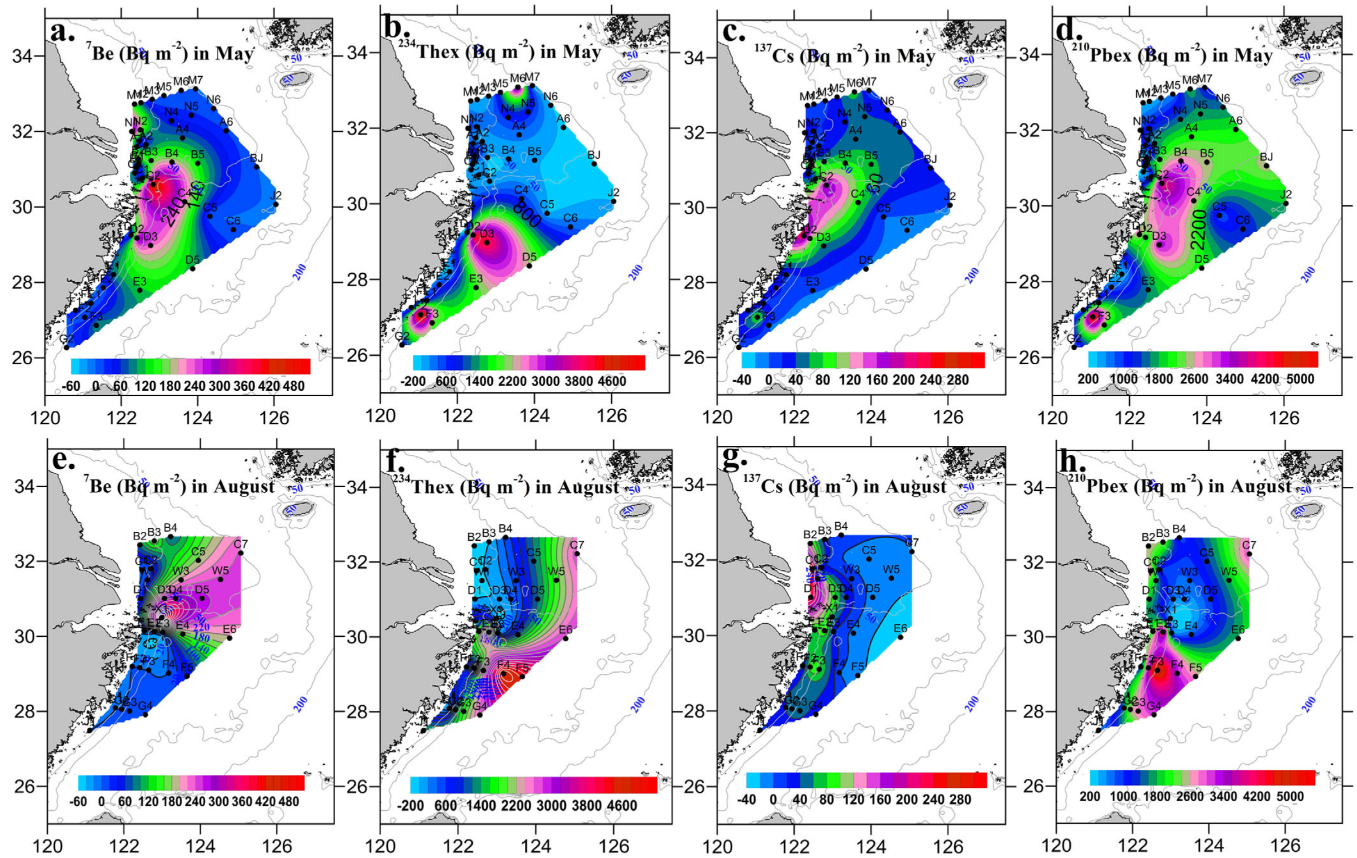


**Figure 7.** Spatial distribution of the $^{7}$Be, $^{234}$Th$_{ex}$, $^{137}$Cs, and $^{210}$Pbex inventories (Bq m$^{-2}$) of MM in May and August.

a residence time of 3.3 ± 2.9 for May and 6.1 ± 5.9 years for August, respectively. This implies that 16–30% of the atmospheric fallout $^{210}$Pb and associated MM is removed due to long-term deposition (or sediment burial) in the study area, assuming that there is no net import or export of MM into the study area. This estimate is based on an assumption, that the amount of $^{210}$Pb produced from the decay of $^{222}$Rn in the water column are negligible compared to the atmospheric fallout component. An inherent assumption is that the MM serves as the source of sediments for the long-term sedimentation. The time scale on the residence time of MM is useful as multiple cycles of deposition-resuspension-transport-deposition-resuspension will significantly impact the biogeochemical cycles of key species that are required in the ecosystem, including both macro and micronutrients.

### 4.4. $^{137}$Cs in MM As a Tracer of the Transport of MM in the ECS

The geochemical behavior of $^{137}$Cs is strikingly different between freshwater and seawater. $^{137}$Cs is highly soluble ($K_d < 500$) and very weakly particle reactive in marine waters and traces the water mass [*Cochran et al.*, 1995; *Smith et al.*, 1999; *Delfanti et al.*, 2003], whereas it is highly particle reactive in freshwater, with $K_d$ values of $10^4-10^6$ cm$^3$ g$^{-1}$ [e.g., *Baskaran et al.*, 2015]. This difference between freshwater and seawater is mainly due to differences in the concentrations of K in these waters. The dating of sediments in estuarine, coastal, and shelf waters are problematic, although several attempts have been made to obtain chronological information from the marine system [e.g., *Su and Huh*, 2002; *Jha et al.*, 2003; *Madsen et al.*, 2005]. However, none of these studies obtained a $^{137}$Cs profile similar to the global fallout cure.$^{137}$Cs have been widely used as a chronometer in freshwater systems [e.g., *Evans et al.*, 1983; *Davis et al.*, 1984; *Baskaran et al.*, 2014, 2015]. The majority of the sedimentary particulate matter discharged by the Changjiang River are "tagged" with $^{137}$Cs and deposited mostly in the nearshore closest to the river mouths. A relatively small fraction (20–30%) is transported to the outer shelf of the ECS [*Qin and Li*, 1983]. A large portion of material deposited nearshore is subsequently resuspended and carried by coastal currents, mainly in the form of MM. For example, in the northeast ECS, a thick layer of MM is observed due to anticlockwise coastal circulation [*Hu and Yang*, 2001]. Cs has been reported to have higher tightly associated sites of layered illite clay minerals due to more tightly associated sites compared to kaolinite and chlorite

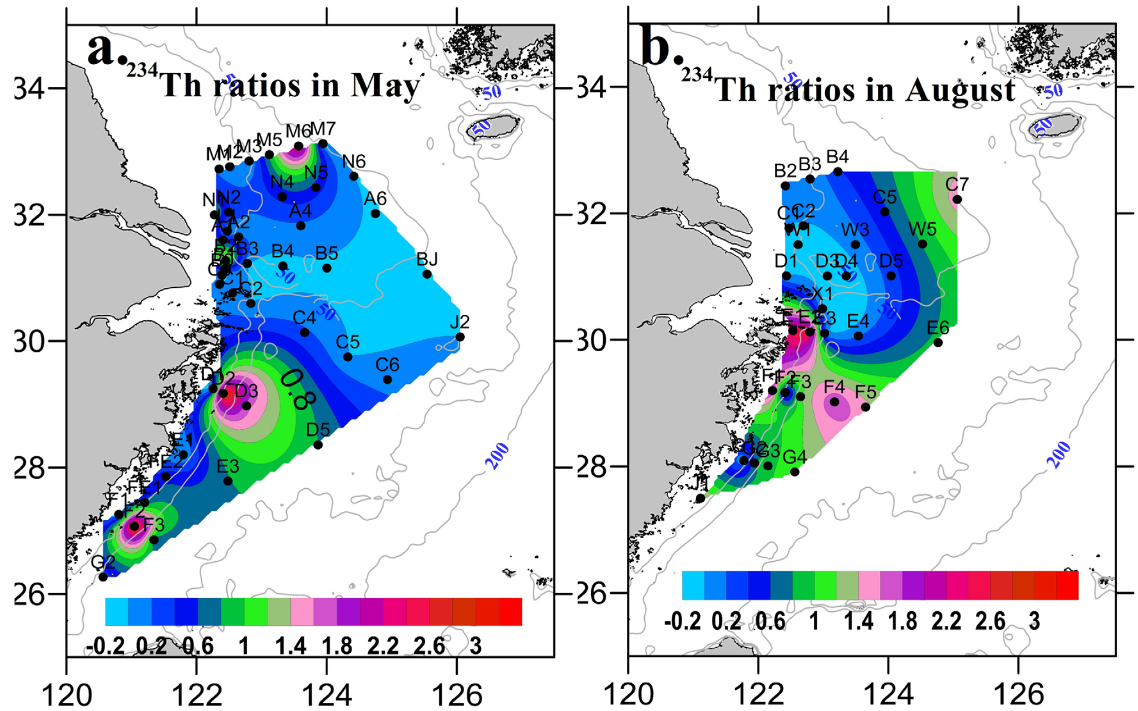


**Figure 8.** Spatial distribution of the $^{234}Th_{ex}$ ratio of MM in May and August. The ratio refers to the ratio of measured excess $^{234}Th$ to that of the water-column-supported $^{234}Th$ inventory in the sediments.

[*Ohnuki and Kozai*, 2013]. Even leaching with 1 *M* HCl of $^{137}Cs$-laden illite resulted in desorption of $<20\%$ [*Ohnuki and Kozai*, 2013]. It has been demonstrated that illite is the most abundant clay mineral (65%–75%) present in the Changjiang River mouth [*Lan et al.*, 2012; *Wang and Yang*, 2013]. Thus, the finer fraction (mainly clay and finer silt) of Changjiang River-derived, $^{137}Cs$-tagged sedimentary matter could serve as an effective tracer of its source in marine environments and support our hypothesis that the activity and inventory of $^{137}Cs$ in MM decreases from the coastal area to the shelf (Figure 5). In the sediment cores, we did not observe a discernible peak in the vertical profiles of $^{137}Cs$, similar to the data presented by [*Huh and Su*, 1999; *Su and Huh*, 2002] on sediment cores analyzed from the ECS. The majority of the oceanic $^{137}Cs$ remains in the dissolved form in the water column, whereas the river-derived $^{137}Cs$ (both dissolved and particulate) is mainly deposited in the nearshore closest to the river mouths. The inventory of $^{137}Cs$ of seawater was reported to be larger than that in underlying sediments in the ECS (i.e., station CB-17, 227 Bq m$^{-2}$ $>$ 203 Bq m$^{-2}$) [*Nagaya and Nakamura*, 1992]. The spatial distribution of $^{137}Cs$ inventory is highly similar to the thickness of MM (positive linear relationship, $R = 0.92$, $p < 0.05$), further demonstrating that $^{137}Cs$ is a suitable tool to trace the transportation of MM which was mainly derived from the Changjiang River input.

### 4.5. Source and Transportation Pathway of the MM

The sources, transport processes, and deposition/resuspension of sediments are among the important components of the study of estuaries, coastal sedimentology, and topography. These resuspension/redeposition processes can affect the early diagenetic environment of sediments, enhanced nitrification of seabed and bottom water: denitrification coupling and nitrogen loss [*Aller*, 1998; *Aller et al.*, 2004]. MM can also carry the organic matter from estuary areas to offshore, supporting nutrients for the marine benthos [*Bianchi et al.*, 2006; *Fabres et al.*, 2008; *Lorenzoni et al.*, 2009]. Due to the seasonal variation of the CDW, the thickness, $^{7}Be$ and $^{137}Cs$ inventories of MM are highest in the north during August and second highest in the south during May, which implies that the Changjiang-loaded materials can be seasonally transported to form the MM in the ECS. The decreasing trend of the inventories of $^{7}Be$ and $^{137}Cs$ from the coast to offshore indicate that the MM was transported from the inshore to outer shelf. Nevertheless, the inventories of $^{210}Pb_{ex}$ and $^{234}Th_{ex}$ were highest in the south of the study area, and previous studies have reported that Pu in the ECS can also be transported from the Pacific Proving Grounds [*Wang and Yamada*, 2005; *Liu et al.*, 2011], suggesting that materials were also transported from the open sea contributing to the formation of MM. In the north offshore, the distribution pattern of $^{7}$Be inventories in August indicates that the riverine materials can also be transported northeastward to this region influenced by the CDW. The materials from the old Huanghe River can be transported to this study area [*Wang et al.*, 2009]. The bimodel distribution of grain size frequency reflect the mixture of materials in two different sources, with the particle size increasing from north to south, suggesting transport from the Yellow Sea to the ECS. Thus, the high $^{7}$Be inventory in August and the bimodel distribution of the grain size frequency indicate that the source of materials in the north offshore is a result of mixing of the old Huanghe River and Changjiang River inputs.

## 5. Summary

From the spatial distribution of MM area, and the activities and inventories of $^{7}$Be, $^{234}$Th$_{ex}$, $^{210}$Pb$_{ex}$, and $^{137}$Cs from a suite of MM samples collected during two seasons in the ECS, we draw the following conclusions:

1. The MM thickness in May and August varied by an order of magnitude, 0.5–7.0 cm (average: 2.2 cm) and from 0.5 to 11 cm (average: 3.9 cm), respectively. The granulometric composition of MM was mainly fine grain size ($>$95% clay + silt, and $<$5% sand) and high porosity ($\geq$0.50), except for several offshore locations, where the MM was sandy, likely due to the presence of relict sediment deposits.
2. The estimated mass of MM in the ECS was 7.8 $\times$ 10$^{8}$ t in May and 8.8 $\times$ 10$^{8}$ t in August; and these values are approximately 4 times higher than the annual sediment discharge from the Changjiang River. Using a simple mass balance calculation of the mass of MM and activity of $^{210}$Pb$_{ex}$, the residence time of MM was estimated to be 3–6 years. This residence time indicates that the MM undergoes multiple cycles of deposition-resuspension-transport-deposition over a period of 3–6 years before eventual burial and/or transport off the shelf. Thus, the MM is expected to play a major role in the biogeochemical cycles of carbon and nutrients in the coastal and shelf regions of the river-dominated marginal seas.
3. The inventories of $^{137}$Cs were significantly higher near the Changjiang estuary and the coastal belt due to $^{137}$Cs-laden terrigenous particulate matter brought by the riverine input. Spatial and temporal variations of the inventories of $^{137}$Cs could be effectively utilized as a transport tracer of MM in river-dominated estuaries and coastal areas around the world.
4. The inventories of $^{7}$Be and the thickness of MM were higher near the river mouth in spring, which is attributed to the higher amount of $^{7}$Be depositional flux and discharge of $^{7}$Be-laden riverine sediment load. The ratio of the measured sediment inventory of $^{234}$Th$_{ex}$ to the production rate in the overlying water column of $>$2.5 in the south inshore during both cruises indicates that sediment focusing resulted in an increased mass flux, which may have been associated with current circulation.
5. Materials of MM near the estuary and along the coast were mainly derived from the Changjiang River input, and the inventories of $^{7}$Be, $^{137}$Cs from the coast to offshore indicate that the MM was transported from inshore to the outer shelf. In the north offshore, the high $^{7}$Be inventory in August and bimodel distribution of grain size frequency indicate that the MM materials in this area were derived from the terrigenous input flowing through the estuary (including the Changjiang River and the old Huanghe River).

**Acknowledgments**
The data reported in this paper can be obtained by contacting the corresponding author Jinzhou Du (jzdu@sklec.ecnu.edu.cn). This research was funded by the Ministry of Science and Technology of PR China (2011CB409801) and Natural Science Foundation of China (41021064). One of the authors, Mark Baskaran, thanks the support from the "High-end Foreign Experts Recruitment Program" sponsored by the State Administration of Foreign Affairs (P.R. China).

## References

Aller, R. C. (1998), Mobile deltaic and continental shelf muds as suboxic, mobileized bed reactors, *Mar. Chem.*, *61*, 143–155.

Aller, R. C., C. Heilbrun, and C. Panzeca (2004), Coupling between sedimentary dynamics, early diagenetic processes, and biogeochemical cycling in the Amazon-Guiznzs mobile mud belt: Coastal French Guiana, *Mar. Geol.*, *208*, 331–360.

Baskaran, M., and A. S. Naidu (1995), $^{210}$Pb-derived chronology, and the fluxes of $^{210}$Pb and $^{137}$Cs isotopes into continental shelf sediments, East Chukchi Sea, Alaskan Arctic, *Geochim. Cosmochim. Acta.*, *59*, 4435–4448.

Baskaran, M., M. Ravichandran, and T. S. Bianchi (1997), Cycling of $^{7}$Be and $^{210}$Pb in a high DOC, shallow, turbid estuary of southeast Texas, *Estuarine Coastal Shelf Sci.*, *45*, 165–176.

Baskaran, M., J. Nix, C. Kuyper, and N. Karunakara (2014), Problems with the dating of sediment core using excess $^{210}$ Pb in a freshwater system impacted by large scale watershed changes, *J. Environ. Radioact.*, *138*, 355–363.

Baskaran, M., C. J. Miller, A. Kumar, E. Andersen, J. Hui, J. P. Selegean, C. T. Creech, and J. Barkach (2015), Sediment accumulation rates and sediment dynamics using five different methods in a well-constrained Dam: Case study from Riley Dam, Michigan, *J. Great Lakes Res.*, *41*(2) 607–617.

Bianchi, T. S., M. A. Allison, E. A. Canuel, D. R. Corbett, B. A. Mckee, S. G. Wakeham, and E. J. Waterson (2006), Rapid export of riverine- and shelf-derived organic matter into the Mississippi canyon, *Eos Trans. AGU*, *87*, 565–573.

Bianchi, T. S., J. J. Galler, and M. A. Allison (2007), Hydrodynamic sorting and transport of terrestrially derived organic carbon in sediments of the Mississippi and Atchafalaya Rivers, *Estuarine Coastal Shelf Sci.*, *73*, 211–222.

Chen, Z., B. Song, Z. Wang, and Y. Cai (2000), Late Quaternary evolution of the sub-aquedus Changjiang Delta, China: Sedimentation, slratigraphy, palynology and deformation, *Mar. Geol.*, *162*, 423–441.

Chert, J. Y., H. F. Zhu, Y. F. Dong, and J. M. Sun (1985), Development of the Changiiang Estuary and its submerged delta, *Cont. Shelf Res.*, *4*(1/2), 47–56.

Cochran, J. K., D. J. Hirschberg, H. D. Livingston, K. O. Buesseler, and R. M. Key (1995), Natural and anthropogenic radionuclide distributions in the Nansen Basin, Arctic Ocean: Scavenging rates and circulation timescales, *Deep Sea Res., Part II*, *42*, 1495–1517.

Corbett, D. R., B. Mckee, and D. Duncan (2004), An evaluation of mobile mud dynamics in the Mississippi Riverdeltaic region, *Mar. Geol.*, *209*, 91–112.

Dai, Z., and J. T. Liu (2013), Impacts of large dams on downstream fluvial sedimentation: An example of the Three Gorges Dam (TGD) on the Changjiang (Yangtze River), *J. Hydrol.*, *480*, 10–18.

Dai, Z., J. Liu, W. Wei, and J. Chen (2014a), Detection of the Three Gorges Dam influence on the Changjiang (Yangtze River) submerged delta, *Sci. Rep.*, *4*, 6600, doi:10.1038/srep06600.

Dai, Z. J., J. T. Liu, H. L. Xie, and W. Y. Shi (2014b), Sedimentation in the outer Hangzhou bay, China: The influence of Changjiang sediment load, *J. Coastal Res.*, *30*(6), 1218–1225.

Davis, R. B., C. T. Hess, S. A. Norton, D. W. Hanson, K. D. Hoagland, and D. A. Anderson (1984), $^{137}$Cs and $^{210}$Pb dating of sediments from soft-water lakes in New England (U.S.A.) and Scandinavia, a failure of $^{137}$Cs dating, *Chem. Geol.*, *44*, 151–185.

Delfanti, R., B. Klein, and C. Papucci (2003), Distribution of $^{137}$Cs and other radioactive tracers in the eastern Mediterranean: Relationship to the deepwater transient, *J. Geophys. Res.*, *108*(C9), 8108, doi:10.1029/2002JC001371.

DeMaster, D. J., S. A. Kuehl, and C. A. Nittrouer (1986), Effects of suspended sediments on geochemical processes near the mouth of the Amazon River: Examination of biological silica uptake and the fate of particle-reactive elements, *Cont. Shelf Res.*, *6*, 107–125.

Du, J., J. Zhang, J. Zhang, and Y. Wu (2008), Deposition patterns of atmospheric $^{7}$Be and $^{210}$Pb in coast of East China Sea, Shanghai, China, *Atmos. Environ.*, *42*, 5101–5109.

Du, J., Y. Wu, D. Huang, and J. Zhang (2010), Use of $^{7}$Be,$^{210}$Pb and $^{137}$Cs tracers to thetransport of surface sediments of the Changjiang Estuary, China, *J. Mar. Syst.*, *82*(4), 286–294.

Du, J., J. Du, M. Baskaran, Q. Bi, D. Huang, and Y. Jiang (2015), Temporal varations of atmospheric depositional fluxes of $^{7}$Be and $^{210}$Pb over 8 years (2006-2013) at Shanghai, China, and synthesis of global fallout data, *J. Geophys. Res. Ocenas*, *120*, 4323–4339, doi:10.1002/2014JD022807.

Evans, D. W., J. L. Alberts, and R. A. Clark (1983), Reversible ion-exchange fixation of cesium-137 leading to mobilization from reservoir sediments, *Geochim. Cosmochim. Acta.*, *47*, 1041–1049.

Fabres, J., T. Tesi, J. Velez, F. Batista, C. Lee, A. Calafat, S. Heussner, A. Palanques, and S. Miserocchi (2008), Seasonal and event-controlled export of organic matter from the shelf towards the Gulf of Lions continental slope, *Cont. Shelf Res.*, *28*, 1971–1983.

Feng, H., J. K. Cochran, and D. J. Hirschberg (1999), $^{234}$Th and $^{7}$Be as tracers for the transport and dynamics of suspended particles in a partially mixed estuary, *Geochim. Cosmochim. Acta.*, *63*, 2487–2505.

Fitzgerald, S. A., J. V. Klump, P. W. Swarzenski, R. A. Mackenzie, and K. D. Richards (2001), Beryllium-7 as a tracer of short-term sediment deposition and resuspension in the Fox River, Wisconsin, *Environ. Sci. Technol.*, *35*(2), 300–305, doi:10.1021/es000951c.

Folk, R. L., and W. C. Ward (1957), Brazos river bar: A study in the significance of grain size parameters, *J. Sediment. Petrol.*, *27*(1), 3–26.

Giffin, D., and D. R. Corbett (2003), Evaluation of sediment dynamics in coastal systems via short-lived radioisotopes, *J. Mar. Syst.*, *42*, 83–96.

Guo, Z. G., T. Lin, G. Zhang, Z. S. Yang, and M. Fang (2006), High-resolution depositional records of polycyclic aromatic hydrocarbons in the central continental shelf mud of the East China Sea, *Environ. Sci. Technol.*, *40*, 5304–5311.

Hideshi, F., T. Fukuyama, and Y. Shirato (2007), Depositon of atmospheric $^{137}$Cs in Japan associated with the Asian dust event of March 2002, *Sci. Total Environ.*, *384*, 306–315.

Hu, D., and Z. Yang (2001), *Key Processes in the Ocean Flux of East China Sea [in Chinese]*, China Ocean Press, Beijing.

Huang, D., J. Du, Y. Wu, D. Li, and J. Zhang (2010), Sinking of particulate $^{234}Th_{xs}$, $^{7}$Be and $^{210}$Pbxs in the Changjiang Estuary, China, *Chin. J. Oceanol. Limnol.*, *28*(6), 1152–1159.

Huang, D., J. Du, B. Deng and J. Zhang (2012), Distribution patterns of particle-reactive radionuclides in sediments offeastern Hainan Island, China: Implications for source and transport pathways, *Cont. Shelf Res.*, *57*, 10–17.

Huang, D., J. Du, W. S. Moore, and J. Zhang (2013), Particle dynamics of the Changjiang Estuary and adjacent coastal region determined by natural particle-reactive radionuclides ($^{7}$Be, $^{210}$Pb, and $^{234}$Th), *J. Geophys. Res. Oceans*, *118*, 1736–1748, doi:10.1002/jgrc.20148.

Huh, C.-A., and C.-C., Su (1999), Sedimentation dynamics in the East China Sea elucidated from $^{210}$Pb,$^{137}$Cs and $^{239,240}$Pu, *Mar. Geol.*, *160*, 183–196.

Jha, S. K., S. B. Chavan, G. G. Pandit, and S. Sadasivan (2003), Geochronology of Pb and Hg pollution in a coastal marine environment using global fallout $^{137}$Cs, *J. Environ. Radioact.*, *69*(1–2), 145–157.

Jweda, J., M. Baskaran, E. Van Hees, and L. Schweitzer (2008), Short-lived radionuclides ($^{7}$Be and $^{210}$Pb) as tracers of particle dynamics in a river system in southeast Michigan, *Limnol. Oceanogr.*, *53*(5), 1934–1944.

Kaste, J. M., and M. Baskaran (2011), Meteoric $^{7}$Be and $^{10}$Be as process tracers in the environment, in *Handbook of Environmental Isotope Geochemistry*, edited by M. Baskaran, pp. 61–86, Springer, N. Y.

Kineke, G. C., and R. W. Sternberg (1995), Distribution of fluid muds on the Amazon continental shelf, *Mar. Geol.*, *125*, 193–233.

Lan, X. H., Z. X. Zhang, R. H. Li, Z. B. Wang, X. H. Chen, and Z. X. Tian (2012), Distribution of clay mineral in surface sediments off Yangtze River estuary, *Mar. Sci. Bull.*, *14*(2), 56–67.

Lane, E. W. (1947), Report of the subcommittee on sediment terminology, *Eos Trans. AGU*, *28*(6), 936–938, doi:10.1029/TR028i006p00936.

Lim, D. I., H. S. Jung, J. Y. Choi, S. Yang, and K. S. Ahn (2006), Geochemical compositions of river and shelf sediments in the Yellow Sea: Grain-size normalization and sediment provenance, *Cont. Shelf Res.*, *26*, 15–24.

Liu, J. P., A. C. Li, K. H. Xu, D. M. Velozzi, Z. S. Yang, J. D. Milliman, and D. J. DeMaster (2006), Sedimentary features of the Changjiang River-derived along-shelf clinoform deposit in the East China Sea, *Cont. Shelf Res.*, *26*, 2141–2156.

Liu, J. P., K. H. Xu, A. C. Li, J. D. Milliman, D. M. Velozzi, S. B. Xiao, and Z. S. Yang (2007), Flux and fate of Changjiang River sediment delivered to the East China Sea, *Geomorphology*, *85*, 208–224.

Liu, Z., J. Zheng, S. Pan, W. Dong, M. Yamada, T. Aono, and Q. Guo (2011), Pu and $^{137}$Cs in the Yangtze River Estuary sediments: Distribution and source identification, *Environ. Sci. Technol.*, *45*(5), 1805–1811.

Lorenzoni, L., R. C. Thunell, C. R. Benitez-Nelson, D. Hollander, N. Martinez, E. Tappa, R. Varela, Y. Astor, and F. E. Muller-Karger (2009), The importance of subsurface nepheloid layers in transport and delivery of sediments to the eastern Cariaco Basin, Venezuela, *Deep Sea Res., Part I*, *56*, 2249–2262.

Madsen, A. T., A. S. Murray, T. J. Andersen, M. Pejrup, and H. Breuning-Madsen (2005), Optically stimulated luminescence dating of young estuarine sediments: A comparison with $^{210}$Pb and $^{137}$Cs dating, *Mar. Geol.*, *214*(1–3), 251–268.

McKee, B. A., and M. Baskaran (1999), Sedimentary processes of Gulf of Mexico estuaries, in *Biogeochemistry of Gulf of Mexico Estuaries*, edited by T. Bianchi, J. Pennock, and R. Twilley, pp. 63–85, John Wiley, N. Y.

McKee, B. A., C. A. Nittrouer, and D. J. DeMaster (1983), The concepts of sediment deposition and accumulation applied to the continental shelf near the mouth of the Changjiang River, *Geology*, *11*, 631–633.

Milliman, J. D. (1991), Flux and fate of fluvial sediments and water in coastal seas, in *Ocean Margin Processes in Global Change*, edited by R. Mantoura, J.-M. Martin, and R. Wollast, pp. 69–90, John Wiley, N. Y.

Ministry of Water Resources Changjiang Water Resources Commission (2011), *Changjiang Sediment Bulletin*, Changjiang Press, Wuhan.

Nagaya, Y., and K. Nakamura (1992), $^{239,240}$Pu and $^{137}$Cs in the east China and the Yellow seas, *J. Oceanogr.*, *48*, 23–35.

Ohnuki, T., and N. Kozai (2013), Adsorption behavior of radioactive cesium by non-mica minerals, *J. Nucl. Sci. Technol.*, *50*(4), 369–375.

Qin, Y., and F. Li (1983), Study of influence of sediment loads discharged from the Huanghe River on sedimentation in the Bohai Sea and the Huanghai Sea, in *Proceedings of International Symposium on Sedimentation on the Continental Shelf With Special Reference to the East China Sea*, pp. 83–92, China Ocean Press, Beijing.

Smith, J. N., K. M. Ellis, and T. M. Boyd (1999), Circulation features in the Central Arctic Ocean revealed by nuclear fuel reprocessing tracers from SCICEX 95 and 96, *J. Geophys. Res.*, *104*(C12), 29,663–29,677.

Smoak, J. M., W. S. Moore, and R. C. Thunell (2000), Influence of boundary scavenging andsediment focusing on $^{234}$Th,$^{228}$Th, and $^{210}$Pb fluxes in the Santa Barbara Basin, *Estuarine Coastal Shelf Sci.*, *51*, 373–384.

Su, C.-C., and C.-A. Huh (2002), $^{210}$Pb,$^{137}$Cs and $^{239;240}$Pu in East China Sea sediments: Sources, pathways and budgets of sediments and radionuclides, *Mar. Geol.*, *183*, 163–178.

Su, J. L. (2001), A review of circulation dynamics of the coastal oceans near China, *Acta Oceanol. Sin.*, *23*(4), 1–16.

Wang, Q., and S. Yang (2013), Clay mineralogy indicates the Holocene monsoon climate in the Changjiang (Yangtze River) Catchment, China, *Appl. Clay Sci.*, *74*, 28–36.

Wang, Y., G. Zhi, G. Li, T. Oguchi, and H. Shen (2009), Discrimination in magnetic properties of different-sized sediments from the Changjiang and Huanghe Estuaries of China and its implication for provenance ofsediment on the shelf, *Mar. Geol.*, *260*, 121–129.

Wang, Z. L., and M. Yamada (2005), Plutonium activities and $^{240}$Pu/$^{239}$Pu atom ratios in sediment cores from the East China Sea and Okinawa Trough: Sources and inventories, *Earth Planet. Sci. Lett.*, *233*, 441–453.

Wu, H., B. Deng, R. Yuan, J. Gu, J. Zhu, and J. Zhang (2013), Detiding measurement on transport of the Changjiang-derived Buoyant Coastal Current, *J. Phys. Oceanogr.*, *43*, 2388–2399.

Wu, H., J. Shen, J. Zhu, J. Zhang, and L. Li (2014), Characteristics of the Changjiang Plume and its extension along the Jiangsu Coast, *Cont. Shelf Res.*, *76*, 108–123.

Yang, S. L., I. M. Belkin, A. I. Belkina, Q. Y. Zhao, J. Zhu, and P. X. Ding (2003), Delta response to decline in sediment supply from the Changjiang River: Evidence of the recent four decades and expectations for the next half-century, *Estuarine Coastal Shelf Sci.*, *57*(4), 689–699.

Yang, S. L., J. Zhang, J. Zhu, J. P. Smith, S. B. Dai, A. Gao, and P. Li (2005), Impact of dams on Yangtze River sediment supply to the sea and delta inter-tidal wetland response, *J. Geophys. Res.*, *110*, F03006, doi:10.1029/2004JF000271.

Zhang, Z., Z. Guo, and G. Zhang (2005), Distribution and source of polycyclic aromatic hydrocarbons in the surface sediments of the mud areas in the East China Sea, *Gcoehimica*, *34*(4), 379–386.

Zhu, Z.-Y., J. Zhang, Y. Wu, Y. Zhang, J. Lin, and S. Liu (2011), Hypoxia off the Changjiang (Changjiang River) Estuary: Oxygen depletion and organicmatter decomposition, *Mar. Chem.*, *125*, 108–116.